

# Design of Frequency Reconfigurable Antenna using Metasurface

Navneet Kaur<sup>1</sup>, Jagtar S. Sivia<sup>2</sup> and Rajni<sup>3</sup>

<sup>1</sup>Research Scholar, Punjabi University, Patiala, Punjab, India

<sup>2</sup>Professor, YCoE, Punjabi University Guru Kashi Campus, Talwandi Sabo, Bathinda, India

<sup>3</sup>Professor, Shaheed Bhagat Singh State University (Formerly S.B.S. State Technical Campus), Ferozepur, India

## Abstract

In this paper, the design of frequency reconfigurable low profile antenna using metasurface (FRAMS) is presented for wireless applications. The designed structure incorporates two substrate layers: rectangular patch with feeding line is printed on the upper face and ground plane on the lower face of first substrate whereas, a metasurface (MS) on the upper face of the second substrate. A periodically positioned double split ring-shaped resonator (DSRSR) structure along the x- and y-axis forms the metasurface. The desired frequency reconfigurability is achieved by rotating the meta surface layer. The High Frequency Structure Simulator V15 has been utilized for the designing and analysis of the proposed antenna. The suggested frequency reconfigurable antenna effectively tunes from 4.97 to 6.09 GHz, thus providing a 20.2% fractional tuning range with 1.12 GHz bandwidth.

## Keywords

Frequency reconfigurable antenna, Metasurface, Rectangular patch antenna, Tuning range, Unit cell

## 1. Introduction

Due to the enormous development, profound research, and rapid proliferation of communication technology, wireless devices are continuously supporting several applications at the same time. It is completely unrealistic to support multiple antennas for multiple applications in one system [1-3]. These multiple individual antennas equipped with a carrier possess some drawbacks such as weight issues, system cost, electromagnetic coupling, and multipath effects when communicating, navigating, and guiding a large range of signals. In recent years, Reconfigurable antennas have gained significant attention to efficiently minimize the number of antennas and overcome these problems[4-5]. These antennas offer compact structures with enhanced gain and radiation pattern characteristics in comparison to the conventional single-band and multiple-band antennas [6]. These antennas have proven their usefulness in a variety of applications including cognitive radio, biomedical, IoT, and satellite communications [7-9]. Depending on the relevant application, these antennas have the ability to adjust frequency, pattern, polarization, and a functional combination of all three [1]. Frequency reconfigurable antenna or tunable antenna seems to be a viable solution for achieving better performance and increased flexibility. They are mainly employed in those systems that require a wider bandwidth. These antennas have the dynamic ability to switch between different resonating frequencies without having a significant impact on radiation pattern and polarization. The frequency reconfiguration is usually achieved by physically or electrically modifying the antenna size using switches, impedance loads, or adjustable materials [10]. PIN diodes and varactor diodes are generally used for attaining the electrical mode of reconfiguration. But, their performance degrades due to the requirement of extra biasing circuits and DC sources. The mechanically reconfigurable antenna requires bulky and complex actuators for generating the mechanical motions. Thus, it becomes difficult to adjust the size and shape of these antennas [11].

International Conference on Emerging Technologies: AI, IoT, and CPS for Science & Technology Applications, September 06–07, 2021, NITTTR Chandigarh, India

EMAIL: navsandhu31696@gmail.com (A. 1); jagtarsivian@gmail.com (A. 2); rajni.c123@mail.com (A. 3)

ORCID: 0000-0001-6192-2306 (A. 1); 0000-0001-7649-851X (A. 2); 0000-0003-3380-6468 (A. 3)

©2021 Copyright for this paper by its authors.

Use permitted under Creative Commons License Attribution 4.0 International (CC BY 4.0).



CEUR Workshop Proceedings (CEUR-WS.org)

A metasurface (MS) provides an optimum choice to deal with this kind of problem. A metasurface is generally a type of two-dimensional surface version of metamaterials. This material can produce unique electromagnetic properties by adjusting the shape, size, and arrangement of unit cell structures. Thus, introducing MS into reconfigurable antennas can help us to achieve multiple reconfigurations [4]. Many frequency reconfigurable antenna designs have been studied in the available literature. Zhu et. al. [12] reported the designing process of frequency reconfigurable metasurface antenna using rectangular loop-shaped unit cells. Zhu et. al. [13] presented a design of frequency reconfigurable slot antenna with a bidirectional radiation pattern. Zhu et. al. [14] evaluated the performance of frequency reconfigurable antenna designed using elliptically-shaped unit cells. Chatterjee et. al. [11] demonstrated the metasurface incorporated frequency reconfigurable slot antenna using meandered unit cells positioned along the x- and y-axis. Chen et. al. [15] achieved reconfigurable frequency and polarization antenna using double layer metasurface structure. Li et. al. [16] investigated the performance of frequency reconfigurable antenna enabled by metasurface and is based on a radially homogenous model.

This paper aims to discuss the design of a metasurface based frequency reconfigurable antenna possessing wide bandwidth and tuning range. The designing methodology for the suggested antenna is elaborated in Section 2. Section 3 elucidates the results and discussion part. In the end, the conclusion is presented in Section 4.

## 2. Antenna Geometry

The geometrical pattern of double layered structure of the FRAMS is depicted in Figure 1. Rogers RO4350B substrate material with a thickness of 1.524 mm is used to design the antenna. The dielectric loss tangent ( $\tan \delta$ ) and relative permittivity ( $\epsilon_r$ ) of the substrate are 0.0037 and 3.48, respectively. Due to the prominent features such as excellent dimensional stability and low loss, Rogers RO4350B substrate material is used in the design. A rectangular patch with side dimensions ( $P_1$ ,  $P_w$ ) and a circular ground plane with a diameter ( $D$ ) is implemented on the upper and lower face of the first substrate layer as shown in Figure 1 (a). To achieve excellent impedance matching, the suggested antenna is excited by a  $50 \Omega$  microstrip feed line. The periodically arranged DRSR unit cells constituting the MS are mounted on the upper face of the second substrate layer as shown in Figure 1 (b). The enlarged structure of the unit cell and a side view showing two substrate layers is elucidated in Figure 1(c) and Figure 1(d), respectively. The desired frequency reconfigurability is obtained by rotating this metasurface layer. The direction of rotation angle ( $\theta_r$ ) possesses equal symmetry along horizontal and vertical directions. Thus,  $\theta_r = -\theta_r$  and the maximum rotation angle considered is  $90^\circ$ .

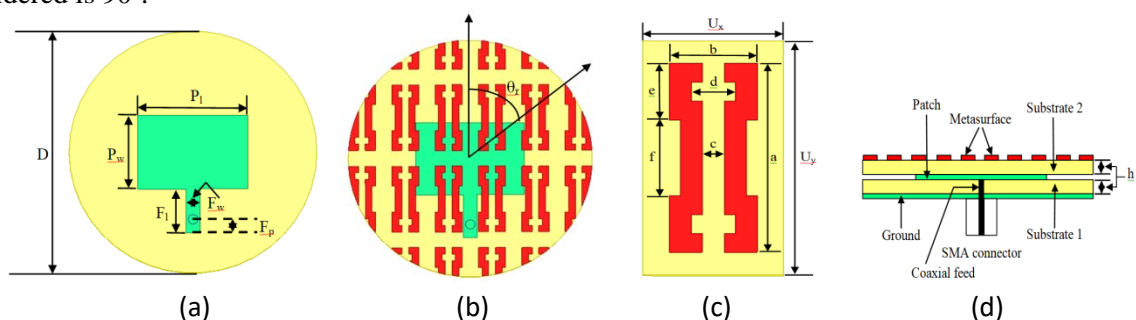


**Figure 1:** Geometrical pattern of FRAMS (a) patch antenna (b) metasurface (c) enlarged unit cell and (d) side view of suggested antenna

**Table 1**

Geometrical dimensionality of FRAMS (mm)

Parameters	D	P <sub>1</sub>	P <sub>w</sub>	F <sub>1</sub>	F <sub>w</sub>	F <sub>p</sub>	g	h
Dimensions	36	16	11	6.5	2	2	2.4	1.524
Parameters	U <sub>y</sub>	U <sub>x</sub>	A	b	c	d	e	f
Dimensions	12.4	6.4	10	4	1	2	3	4

The reliable and commercially available Ansoft's three-dimensional, finite element method (FEM) based HFSS solver is used for performing the electromagnetic simulations and obtaining the resonance characteristics in SRR structures [17]. The unit cell is placed inside a simulation model for characterizing the metamaterial properties. Each simulation model consists of a dual-port waveguide mode with perfect electric (PE) and perfect magnetic (PM) conductor boundaries assigned along appropriate wall pairs. A dielectric slab is placed at the center of the waveguide set up [18]. Waveports are applied along both sides from  $-x$  to  $+x$ . The values of transmission ( $S_{21}$ ) and reflection ( $S_{11}$ ) coefficient are obtained from this arrangement. From Figure 2, it is revealed that a strong reflection of  $-32.26$  dB is observed at  $7.97$  GHz. This frequency corresponds to the resonance of the left-handed metamaterial (LHM) structure. Resonance occurs at a frequency that is similar to the frequency where the logarithmic transmission has the lowest value. The minimum value of the first transmission of the proposed structure is  $-54.50$  dB at  $8.93$  GHz [19]. The magnitude and phase of  $S_{11}$  and  $S_{21}$  are illustrated in Figure 3. The metamaterial behavior is determined from the phase reversal behavior of  $S_{11}$  and  $S_{21}$  at a particular frequency. Figure 4 shows the real and imaginary values of both coefficients that are further used to evaluate the negative characteristics of permeability and permittivity.

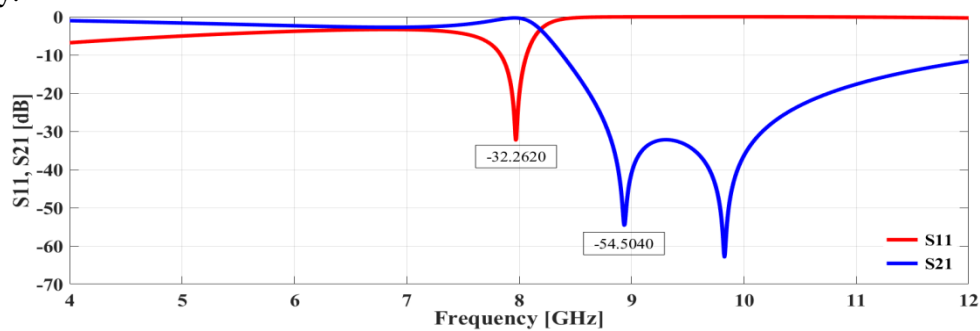


**Figure 2:** Reflection ( $S_{11}$ ) and transmission ( $S_{21}$ ) coefficient of unit cell

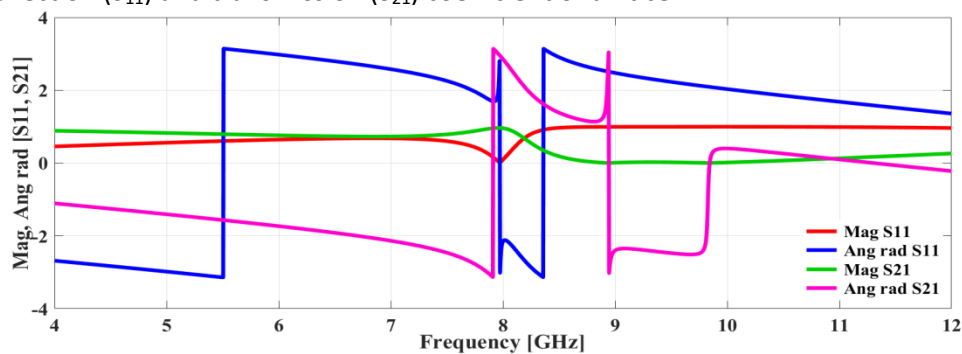


**Figure 3:** Magnitude and phase of the unit cell

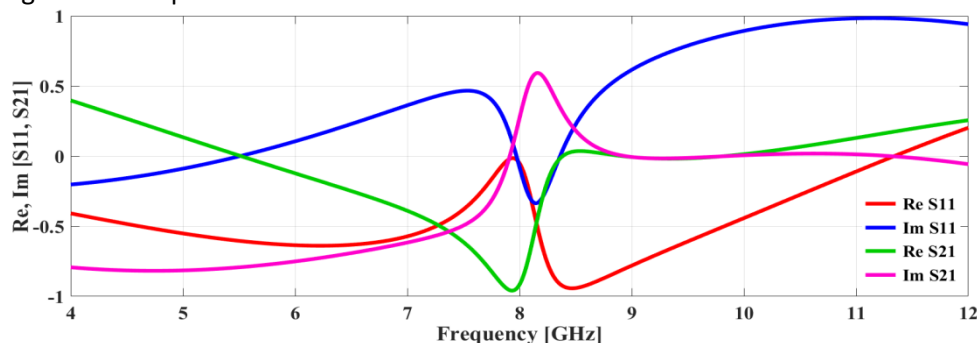


**Figure 4:** Real and imaginary parts of the unit cell

A standard and robust method called Nicolson-Ross-Weir (NRW) approach is used for measuring the effective values of homogenous parameters [20]. It is a commonly used technique that characterizes the electromagnetic properties of metamaterials [21]. It starts with the introduction of composite terms.

$$V_1 = S_{21} + S_{11} \quad (1)$$

$$V_2 = S_{21} - S_{11} \quad (2)$$

$$\mu_r = \frac{2}{jk_0 d} \frac{1 - V_2}{1 + V_2} \quad (3)$$

$$\epsilon_r = \frac{2}{jk_0 d} \frac{1 - V_1}{1 + V_1} \quad (4)$$

where,  $V_1$  and  $V_2$  are the combined terms describing the sum and difference of  $S_{11}$  and  $S_{21}$ , respectively.  $k_0$  symbolizes the free space wave number,  $d$  represents the substrate thickness,  $\mu_r$  and  $\epsilon_r$  signify the relative permeability and permittivity, respectively.

The MATLAB script is then generated using the expressions given in mathematical formulations to derive the complex permittivity and permeability curves. Figure 5 (a) and Figure (b) show the real and imaginary values of extracted permeability and permittivity, respectively. From these figures, it is revealed that these parameters are simultaneously negative in 7.94 to 8.5 GHz which is the required frequency region of interest.

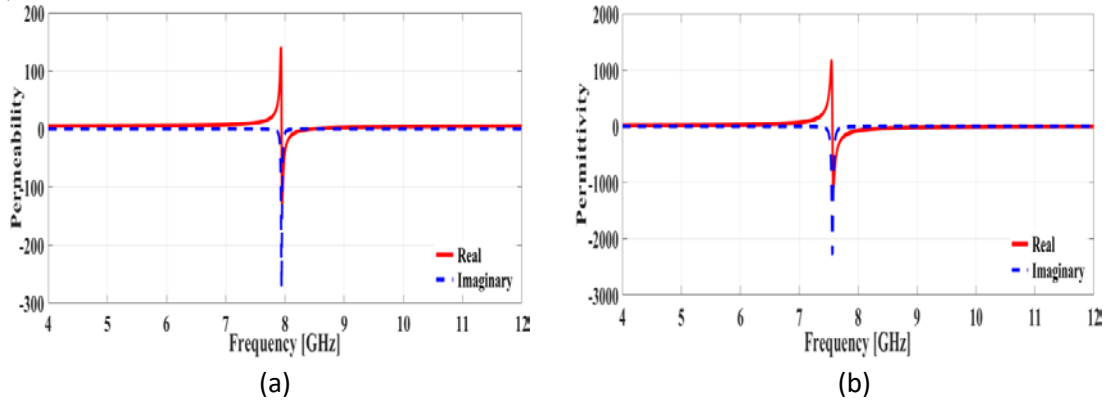


Figure 5: Extracted real and imaginary values of (a) permeability, and (b) permittivity

### 3. Results and Discussions

#### 3.1 Frequency Reconfigurability

The reflection coefficient is an important performance parameter that judges the frequency reconfigurability operation of an antenna. It has been clearly illustrated from Figure 6 that as  $\theta_r$  changes from  $0^\circ$  towards  $30^\circ$ ,  $60^\circ$ , and  $90^\circ$ , the resonant frequency shifts its value from 4.97 to 6.09 GHz with 20.2% fractional tuning range and 1.12 GHz bandwidth. The best matching condition is observed at a 5.92 GHz value that corresponds to  $60^\circ$  angle. As  $\theta_r$  further increases, the resonant frequency decays. The frequency range chosen for the operation is 4.5 GHz to 6.5 GHz.

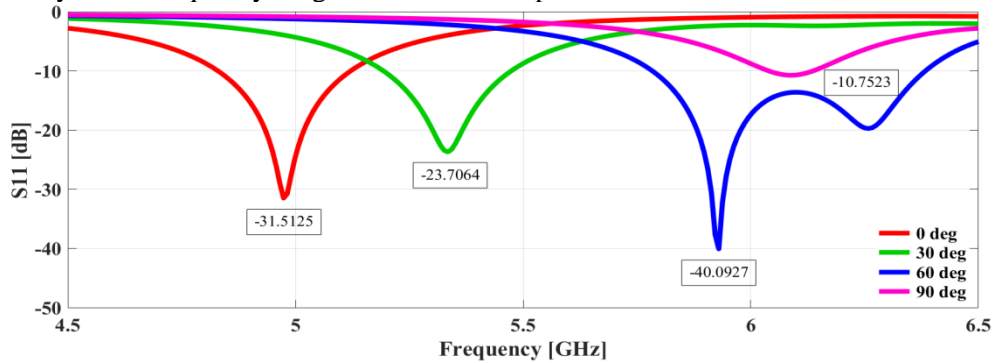
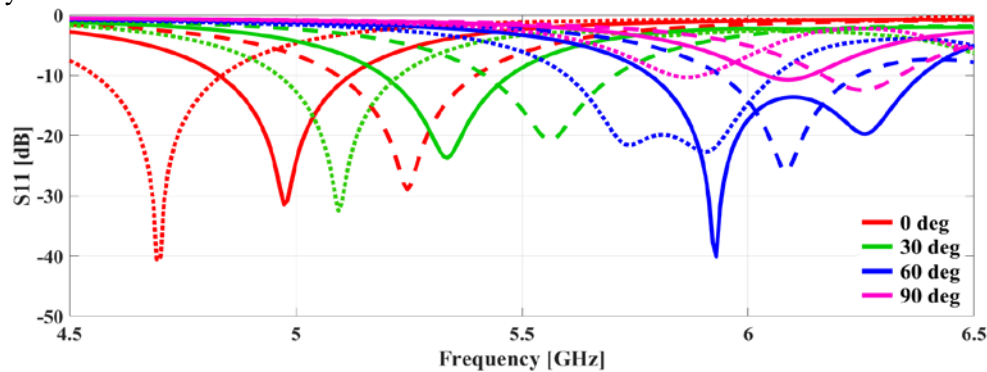
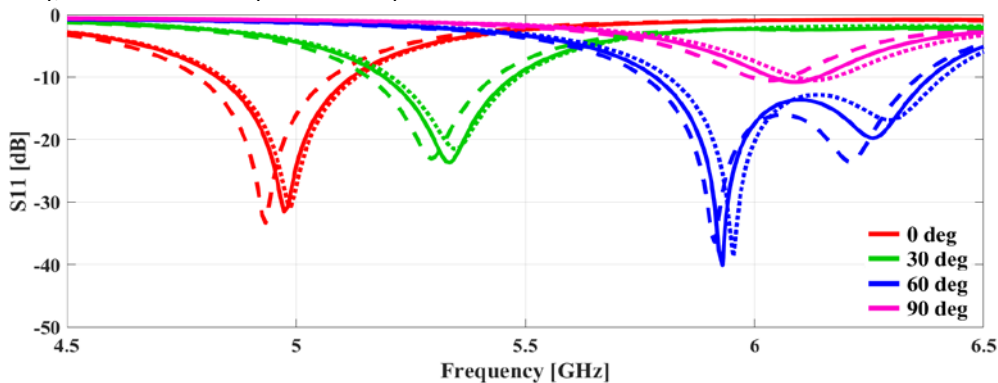


Figure 6:  $S_{11}$  for  $\theta_r = 0^\circ, 30^\circ, 60^\circ, \text{ and } 90^\circ$

Parametric analysis is done to evaluate the effect of important geometrical parameters such as ‘a’, ‘b’, and ‘g’ on the performance of an antenna. These parameters play a vital role in designing the antenna and are varied with a step size of 1mm. The effect of parameter ‘a’ on the performance of an antenna is elucidated in Figure 7. As the value of parameter ‘a’ decreases from 10 to 9 mm, the resonant frequency moves along the upper side whereas, as the value increases from 10 to 11 mm, the resonant frequency moves along the lower side. The effect of parameter ‘b’ on the resonant frequency is illustrated in Figure 8. When the value of ‘b’ is changed from 4 to 3 mm, a slight shift towards the left side is observed and on increasing the value of ‘b’ from 4 to 5 mm, the resonant frequency shifts slightly towards the right side of the original curve. Figure 9 depicts the effect of parameter ‘g’ on the antenna performance. The resonant frequency shifts towards the left side on decreasing the value of ‘g’ to 1.4 mm and the right side on increasing the value to 3.4 mm. From the abovementioned parametric analysis, the optimal values of parameters ‘a’, ‘b’, and ‘g’ are 10 mm, 4 mm, and 2.4 mm, respectively.



**Figure 7:** Effect of parameter ‘a’ on the antenna performance when a = 9 mm (dashed line), a = 10 mm (solid line), and a = 11 mm (dotted line)



**Figure 8:** Effect of parameter ‘b’ on the antenna performance when b = 3 mm (dashed line), b = 4 mm (solid line), and b = 5 mm (dotted line)

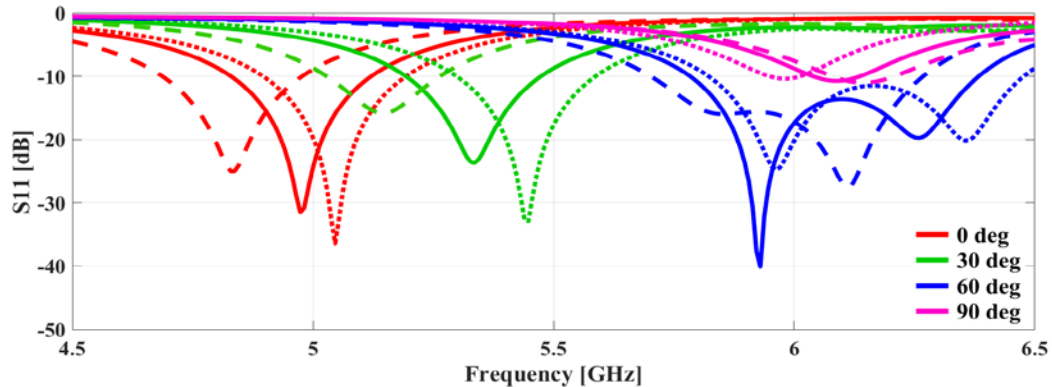


**Figure 9:** Effect of parameter ‘g’ on the antenna performance when g = 1.4 mm (dashed line), g = 2.4 mm (solid line), and g = 3.4 mm (dotted line)

Voltage standing wave ratio (VSWR) is an important performance parameter since it is linked to the reflection coefficient that in turn leads to the impedance matching. There will be poor impedance matching if a larger mismatch is observed between VSWR and the reflection coefficient. As a result, VSWR for antenna should be  $\leq 2$  to achieve acceptable impedance matching [22]. The VSWR at different rotation angles is illustrated in Figure 10. From this Figure, it is noticed that observed VSWR is 1.0546, 1.1396, 1.0200, and 1.8169 corresponding to  $0^\circ$ ,  $30^\circ$ ,  $60^\circ$ , and  $90^\circ$  rotation angles. The minimum value of VSWR at  $60^\circ$  indicates the best matching of impedance.

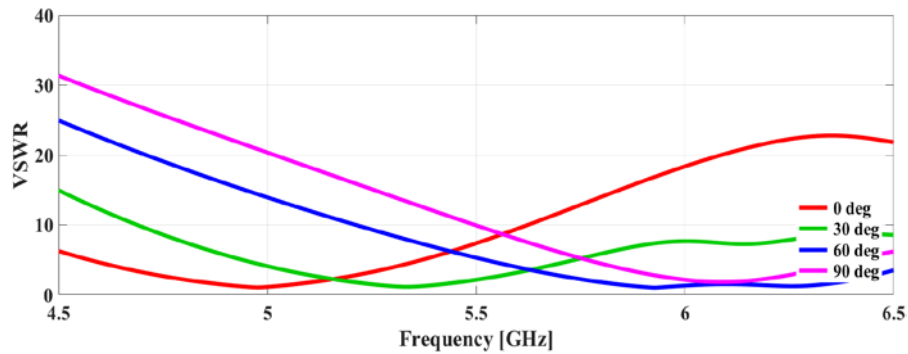


Figure 10: VSWR at different rotation angles

### 3.2 Radiation Pattern

The radiation pattern of FRAMS at  $\theta_r = 0^\circ$ ,  $30^\circ$ ,  $60^\circ$ , and  $90^\circ$  in correspondence to 4.97 GHz, 5.33 GHz, 5.92 GHz, and 6.09 GHz, respectively are elucidated in Figure 11. It is clearly shown that the observed radiation patterns are quite similar in all of the four states. The x-z plane shows a bidirectional radiation pattern and the y-z plane shows an omnidirectional radiation pattern. This clearly shows that metasurface helps in achieving the desired frequency reconfigurability without affecting the polarization. These plots also indicate that co-polarization is more as compared to cross-polarization resulting in high polarization purity of the designed antenna. The gain of the antenna changes from 5.84 to 6.93 dB in the frequency range of operation.

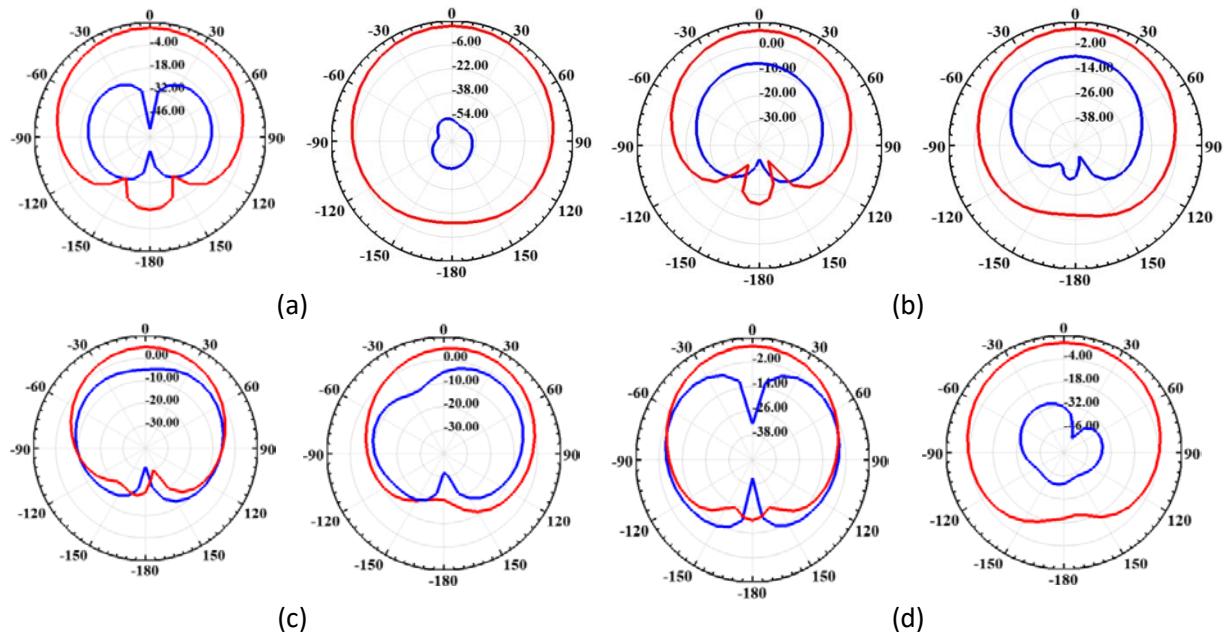


Figure 11: Radiation pattern (a) x-z and y-z plane for  $\theta_r = 0^\circ$  at 4.97 GHz (b) x-z and y-z plane for  $\theta_r = 30^\circ$  at 5.33 GHz (c) x-z and y-z plane at  $\theta_r = 60^\circ$  for 5.92 GHz (d) x-z and y-z plane for  $\theta_r = 90^\circ$

The comparison of the proposed antenna with the other reported antennas is shown in Table 2. It is well understood from the table that the suggested antenna provides higher bandwidth, wider tuning range, and acceptable gain at all resonating frequencies.

**Table 2**  
Comparison of the proposed antenna with the other reported antennas

Ref. No.	[12]	[13]	[11]	[15]	[16]	Proposed antenna
Overall size	40 mm	50 mm	105mmx105mm	-	50 mm	36 mm
Tuning range	4.76-5.51 GHz	2.78-3.2 GHz	1.9-2.3 GHz	4-4.35 GHz	3.97-4.74 GHz, 3.84-4.55 GHz (ellipse) and 3.82-4.87 GHz (wire)	4.97-6.09 GHz
Bandwidth	750 MHz	420 MHz	-	350 MHz	-	1.12 GHz
Fractional Tuning Range	14.6%	14%	19%	8.4%	21.1%, 18.9% (ellipse) and 24.2% (wire)	20.2%
Realized Gain	>5 dBi	4.8 dBi	5 dBi	5 dBi	-	> 5.84 dBi
Reconfigurability type	Freq	Freq	Freq	Freq and Polarization	Freq	Freq

## 4. Conclusion

A rotatable metasurface based microstrip patch antenna with reconfigurable frequency has been designed. The geometry of an antenna consists of a microstrip patch antenna with a circular ground plane and a metasurface designed on a first and second substrate, respectively. It has been studied that by rotating the metasurface structure, the frequency reconfiguration property is achieved. The observed results show that reconfiguration of frequency is attained in the 4.97 to 6.09 GHz range with fractional tuning and bandwidth of 20.2% and 1.12 GHz, respectively.

## 5. References

- [1] A. A. Palsokar, and S. L. Lahudkar, "Frequency and Pattern Reconfigurable Rectangular Patch Antenna using Single PIN diode", *International Journal of Electronics and Communications*, Vol. 125, No. 3, Oct. 2020.
- [2] I. K. Bhangi, J. S. Sivia, "Minkowski and Hilbert Curves Based Hybrid Fractal Antenna for Wireless Applications", *International Journal of Electronics and Communications*, Vol. 85, pp. 159-168, Feb. 2018.
- [3] K. Kaur, J. S. Sivia, "A Compact Hybrid Multiband Antenna for Wireless Applications", *Wireless Personal Communications*, Vol. 97, No. 4, pp. 5917-5927, Dec. 2017.
- [4] A. Chen, and X. Ning, "A pattern and polarization reconfigurable antenna with metasurface", *International Journal of RF and Microwave Computer-Aided Engineering*, pp. 1-11, June 2020.
- [5] N. Kaur, J. S. Sivia, Rajni, "Different Reconfiguration Mechanisms and Applications in Planar Antennas: A Review", *International Conference on Intelligent Communication and Computational Research (ICICCR-2020)*, 25<sup>th</sup> January 2020, Rajpura, Punjab.

- [6] N. Kumar, P. Kumar, and M. Sharma, "Reconfigurable Antenna and Performance Optimization Approach", *Wireless Personal Communications*, Vol. 112, No. 4, pp. 2187-2212, Jan. 2020.
- [7] A. I. Hussain, and A. Z. Sayed, "Optimal User Association of LTE/Wi-Fi/Wi-Gig Bands in 5G Cellular Networks", *International Journal on Semantic Web and Information System (IJSWIS)*, Vol. 17, Issue 2, pp. 22-40, 2021.
- [8] A. Tewari and B. B. Gupta, "Secure Timestamp-Based Mutual Authentication Protocol for IoT Devices Using RFIB Tags", *International Journal on Semantic Web and Information System (IJSWIS)*, Vol. 16, Issue 3, pp. 20-34, July 2020.
- [9] B. Sejdiu, F. Ismaili, and L. Ahmedi, "Integration of Semantics Into Sensor Data for the IoT: A Systematic Literature Review", *International Journal on Semantic Web and Information System (IJSWIS)*, Vol. 16, Issue 4, pp. 1-25, 2020.
- [10] B. Ashvanth, B. Partibane, M. G. N. Alsath, and R. Kalidoss, "Gain enhanced multipattern reconfigurable antenna for vehicular communications", *International Journal of RF and Microwave Computer-Aided Engineering*, Vol. 30, No. 4, pp. 1-16, March 2020.
- [11] J. Chatterjee, A. Mohan, and V. Dixit, "A Novel Frequency Reconfigurable Slot Antenna using Metasurface", *IEEE Indian Conference on Antennas and Propagation (InCAP) 16-19<sup>th</sup> Dec, 2018, Hyderabad, India.*
- [12] H. L. Zhu, X. H. Liu, S. W. Cheung, and T. I. Yuk, "Frequency-reconfigurable antenna using metasurface", *IEEE Transactions on Antennas and Propagation*, Vol. 62, No. 1, pp. 80-85, Jan. 2014.
- [13] H. L. Zhu, S. W. Cheung, X. H. Liu, Y. F. Cao, T. I. Yuk, "Frequency Reconfigurable Slot Antenna using Metasurface", *The 8<sup>th</sup> European Conference on Antennas and Propagation (EuCAP)*, pp. 2575-2577, April 2014, The Hague, Netherlands.
- [14] M. Zhu, and L. Sun, "Design of Frequency Reconfigurable Antenna Based on Metasurface," *IEEE 2<sup>nd</sup> Advanced Information Technology, Electronic, and Automation Control Conference (IAEAC)*, March 2017, Chongqing, China.
- [15] X. Chen, Y. Zhao, "Dual-band polarization and frequency reconfigurable antenna using double layer metasurface", *International Journal of Electronics and Communications*, Vol. 95, pp. 82-87, Oct. 2018.
- [16] H. Li, X. Man, and J. Qi, "Accurate and Robust Characterization of Metasurface-Enabled Frequency Reconfigurable Antennas by Radially Homogeneous Model," *IEEE Access*, Vol. 7, pp. 122605-122612, Sept. 2019.
- [17] J. Y. Chen, W. L. Chen, J. Y. Yeh, L. W. Chen, and C. C. Wang, "Comparative Analysis of Split Ring Resonators for Tunable Negative Permeability Metamaterials based on Anisotropic Dielectric Substrates", *Progress In Electromagnetics Research M*, Vol. 10, pp. 25-38, 2009.
- [18] A. Sethi, and Rajni, "Determination of Electromagnetic Parameters of a New Metasurface Comprising of Square Loop," *Journal of Engineering Science and Technology*, Vol. 13, No. 1, pp. 048-057, 2018.
- [19] Rajni, and A. Marwaha, "Resonance Characteristics and Effective Parameters of New Left Hand Metamaterial," *Telkomnika Indonesian Journal of Electrical Engineering*, Vol. 15, No. 3, pp. 497-503, Sept. 2015.
- [20] E. J. Rothwell, J. L. Frasch, S. M. Ellison, P. Chahal, and R. O. Ouedraogo, "Analysis of the Nicolson-Ross-Weir Method for Characterizing the Electromagnetic Properties of Engineered Materials", *Progress In Electromagnetics Research*, Vol. 157, pp. 31-47, 2016.
- [21] F. Costa, M. Borgese, M. Degiorgi, and A. Monorchio, "Electromagnetic Characterization of Materials by Using Transmission/Reflection (T/R) Devices", *Electronics*, Vol. 6, No. 95, pp. 1-27, 2017.
- [22] G Singh, Rajni and A Marwaha, " Design of G-Shaped Defected Ground Structure for Bandwidth Enhancement ," *International Journal of Computer Applications*, Vol. 75, No. 9, pp. 7-11, August 2013.